

University of Groningen

Comparison of conventional and higher-resolution reduced-FOV diffusion-weighted imaging of breast tissue

Baron, Paul; Wielema, Mirjam; Dijkstra, Hildebrand; Potze, Jan Hendrik; Dorrius, Monique D.; Sijens, Paul E.

Published in:
Magnetic Resonance Materials in Physics, Biology and Medicine

DOI:
[10.1007/s10334-022-01055-x](https://doi.org/10.1007/s10334-022-01055-x)

IMPORTANT NOTE: You are advised to consult the publisher's version (publisher's PDF) if you wish to cite from it. Please check the document version below.

Document Version
Publisher's PDF, also known as Version of record

Publication date:
2023

[Link to publication in University of Groningen/UMCG research database](#)

Citation for published version (APA):

Baron, P., Wielema, M., Dijkstra, H., Potze, J. H., Dorrius, M. D., & Sijens, P. E. (2023). Comparison of conventional and higher-resolution reduced-FOV diffusion-weighted imaging of breast tissue. *Magnetic Resonance Materials in Physics, Biology and Medicine*, 36, 613–619. <https://doi.org/10.1007/s10334-022-01055-x>

Copyright

Other than for strictly personal use, it is not permitted to download or to forward/distribute the text or part of it without the consent of the author(s) and/or copyright holder(s), unless the work is under an open content license (like Creative Commons).

The publication may also be distributed here under the terms of Article 25fa of the Dutch Copyright Act, indicated by the "Taverne" license. More information can be found on the University of Groningen website: <https://www.rug.nl/library/open-access/self-archiving-pure/taverne-amendment>.

Take-down policy

If you believe that this document breaches copyright please contact us providing details, and we will remove access to the work immediately and investigate your claim.

Downloaded from the University of Groningen/UMCG research database (Pure): <http://www.rug.nl/research/portal>. For technical reasons the number of authors shown on this cover page is limited to 10 maximum.



Comparison of conventional and higher-resolution reduced-FOV diffusion-weighted imaging of breast tissue

Paul Baron¹ · Mirjam Wielema¹ · Hildebrand Dijkstra¹ · Jan Hendrik Potze¹ · Monique D. Dorrius¹ · Paul E. Sijens¹

Received: 9 September 2022 / Revised: 11 November 2022 / Accepted: 7 December 2022 / Published online: 17 December 2022
© The Author(s), under exclusive licence to European Society for Magnetic Resonance in Medicine and Biology (ESMRMB) 2022

Abstract

Objective Reduced FOV-diffusion-weighted imaging (rFOV-DWI) allows for acquisition of a tissue region without back-folding, and may have better fat suppression than conventional DWI imaging (c-DWI). The aim was to compare the ADCs obtained with c-DWI bilateral-breast imaging with single-breast rFOV-DWI.

Materials and Methods Breasts of 38 patients were scanned at 3 T. The mean ADC values obtained for 38 lesions, and fibro-glandular ($N=35$) and adipose ($N=38$) tissue ROIs were compared between c-DWI and higher-resolution rFOV-DWI (Wilcoxon rank test). Also, the ADCs were compared between the two acquisitions for an oil-only phantom and a combined water/oil phantom. Furthermore, ghost artifacts were assessed.

Results No significant difference in mean ADC was found between the acquisitions for lesions (c-DWI: $1.08 \times 10^{-3} \text{ mm}^2/\text{s}$, rFOV-DWI: $1.13 \times 10^{-3} \text{ mm}^2/\text{s}$) and fibro-glandular tissue. For adipose tissue, the ADC using rFOV-DWI ($0.31 \times 10^{-3} \text{ mm}^2/\text{s}$) was significantly higher than c-DWI ($0.16 \times 10^{-3} \text{ mm}^2/\text{s}$). For the oil-only phantom, no difference in ADC was found. However, for the water/oil phantom, the ADC of oil was significantly higher with rFOV-DWI compared to c-DWI.

Discussion Although ghost artifacts were observed for both acquisitions, they appeared to have a greater impact for rFOV-DWI. However, no differences in mean lesions' ADC values were found, and therefore this study suggests that rFOV can be used diagnostically for single-breast DWI imaging.

Keywords Diffusion-weighted imaging · Breast cancer · Resolution · Reduced field of view DWI

Introduction

Conventional MR diffusion-weighted imaging (c-DWI) of breast tissue is hindered by its low spatial resolution. This may be partly overcome by reducing the acquired Field Of View (FOV) to only one breast while keeping the same number of phase encoding lines. However, with conventional 2D imaging techniques, this would result in back-folding in the phase encode direction. Although the frequency encode direction is free from back-folding, for single breast imaging, both the AP and RL directions are concerns for back-folding as tissue lies directly outside the FOV (Fig. 1).

Using a 2D radiofrequency (RF) acquisition pulse [1], only a selected volume is excited, allowing for a smaller

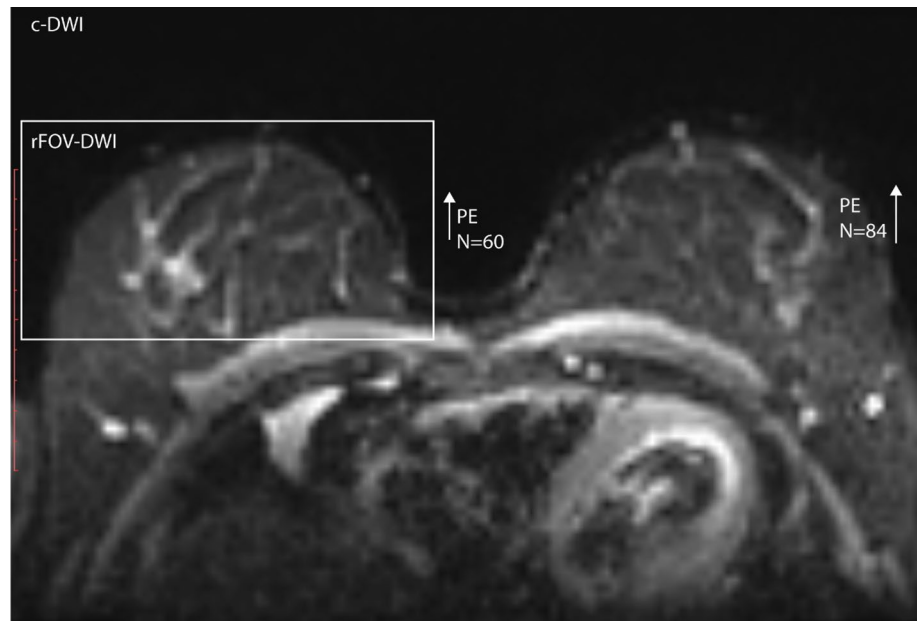
volume to be encoded without back-folding. An additional potential advantage of 2D excitation techniques may be better fat suppression because of reduced B1 and B0 inhomogeneity. A smaller volume in itself may contain less tissue susceptibility variations and thus improved B0 shimming. Furthermore, the 2D RF pulse may be optimized to partly mitigate B1 and B0 inhomogeneity [2]. Disadvantages of 2D RF excitation are generally the longer minimum echo time (TE) as a compromise in the occurrence of side lobe excitations [3]. However, in MRI scanners equipped with multi-channel transmit, the minimum echo time can be reduced using Transmit SENSE techniques [1, 4].

Reduced Field Of View (rFOV) DWI has been applied to multiple tissue regions, including Breast [5], Spinal Cord [6], Prostate [7], Cervix [8], and Brain [9]. The above-mentioned breast study analysis was limited to lesions, without consideration of fibro-glandular and adipose tissue [5]. Because of potential differences in image quality and fat suppression efficacy using rFOV-DWI compared to conventional DWI, the aim of this study was to compare

✉ Paul Baron
P.Baron@umcg.nl

¹ Department of Radiology, University of Groningen, University Medical Center Groningen, Hanzplein 1, 9713 GZ Groningen, The Netherlands

Fig. 1 Illustration of how rFOV was used to decrease the number of phase encoding lines and increase the spatial resolution



ADC values obtained in one breast with both acquisition techniques. This study was part of a larger clinical study, with ADC values obtained for the lesion, fibro-glandular, and adipose regions. Also, oil/water phantom experiments were conducted to study the influence of using a reduced FOV in more detail.

Methods

Patient study

In this prospective IRB approved study, 38 consecutive patients were included with 38 enhancing breast mass lesions of diameter ≥ 0.8 cm (16 malignant: 11 invasive carcinomas, 4 ductile carcinomas in situ, 1 inflammatory breast cancer; 22 benign: 8 adenoses, 6 metaplasia/cystic changes, 5 fibro-adenomas, 2 fibrosis, and 1 Flat epithelial atypia), confirmed by pathology or follow-up.

MR Protocol

All scans were conducted on a 3 Tesla MRI system (Magnetom Skyra, Siemens Medical Solutions, Erlangen, Germany). The subjects were positioned in head-first prone position, and an 18-channel breast coil (Siemens Medical Solutions, Erlangen, Germany) was used for signal reception. All DWI scans were acquired in the axial orientation using a single-shot echo planar imaging (EPI) for readout. The parameters for c-DWI were: FOV = 350×210 mm, $N = 140 \times 84$, ST/gap = 5 mm/20%, no interpolation, 31 slices, TR/TE = 5400/60 ms, and scan time = 1 min

53 s. For rFOV-DWI, the Siemens ZOOMit [10] tool was used, with FOV = 150×91.8 mm, $N = 98 \times 60$, ST/gap = 5 mm/10%, interpolated voxel size = $0.8 \times 0.8 \times 5$ mm, 20 slices, TR/TE = 4300/73 ms, multi-transmit Tx = 1, and scan time = 1 min 36 s. Both acquisitions used spectral adiabatic inversion recovery (SPAIR) for fat suppression, GRAPPA = 2, and three orthogonal diffusion directions with b values 0 (NSA = 1) and 1000 (NSA = 5) s/mm^2 .

To evaluate the SNR with the two protocols, repeated ($N = 8$) DWI ($b = 0$) scans were acquired from one volunteer's breast with both rFOV-DWI and c-DWI. The SNR of fibro-glandular and adipose tissue was calculated as the mean over the repeated DWI magnitude images divided by the standard deviation over the DWI magnitude images.

Patient image analysis

The ADC calculation and ROI drawing were performed in MATLAB (2018, The Mathworks, Natick, MA, USA). The ADC was calculated as:

$$ADC = -\ln\left(\frac{S_{1000}}{S_0}\right) / 1000$$

where S_{1000} and S_0 are the DWI magnitude images at $b = 1000$ and 0 s/mm^2 , respectively. Preference was given to this calculation rather than using the vendor's diffusion package software, which truncates ADC values to 0 for all $ADC < 0$.

Using whole lesion freehand tissue selection (Fig. 2), mean ADCs of c-DWI and rFOV-DWI were calculated. The ROI was drawn on the high $b = 1000$ image, with the DCE

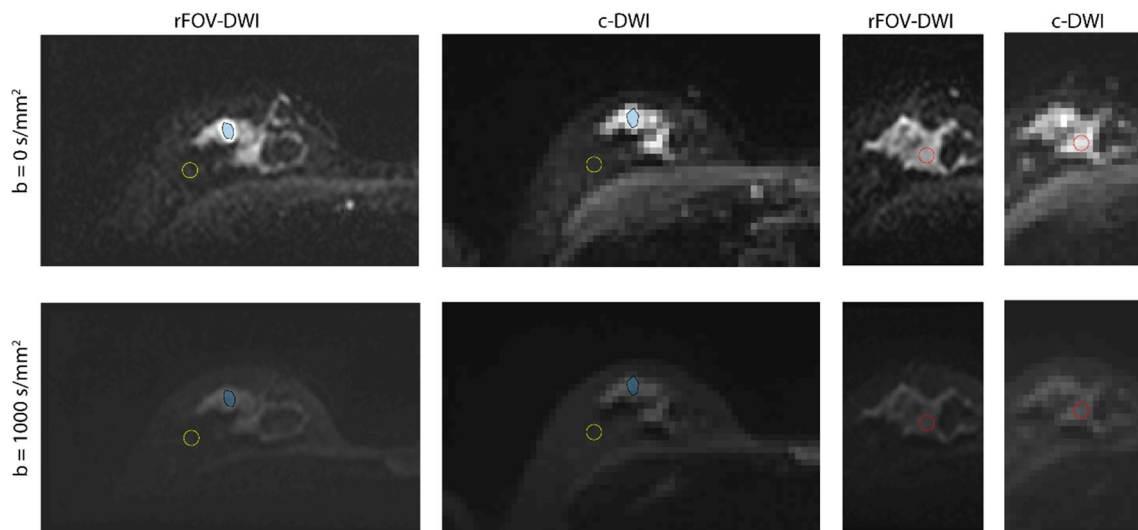


Fig. 2 rFOV-DWI and c-DWI example images for $b=0 \text{ s/mm}^2$ (top row) and $b=1000 \text{ s/mm}^2$ (bottom row). ROIs shown are freehand ROI for the lesion (shaded blue) and circular ROIs for adipose (yellow) and fibro-glandular tissue (red, cropped images on the right side).

perfusion scans (which were acquired in a prior session) used as reference. For fatty ($N=38$) and fibro-glandular ($N=35$, 3 were excluded due to insufficient amount), tissue circular ROIs were used (Fig. 2, diameter = 6 mm). Due to the non-normal distribution median, ADC (\pm IQR) was given, and Wilcoxon rank test was used to compare ADCs. Additionally, the area under the curve of a ROC graph was determined for both acquisition protocols.

Assessment of Image ghost artifacts

The presence of ghost artifacts in the DWI images of the 38 patients was reviewed by one MR physicist (P.B.) with more than 11 years of experience in MRI physics. The reviewer assessed ghost artifacts present in the tissue and air. Differences in noise level, water/fat shift appearance, Gibbs artifacts, and artifacts appearing at the outer edges of the imaging volume were ignored. We defined the artifact score as follows: score 1, no ghost artifacts visible; Score 2, minimally visible either in extent or intensity; Score 3, moderately present either in extent or intensity. Score 4, severe. A Student's t test was used to test for a significant ($p < 0.05$) difference between c-DWI and rFOV-DWI.

Phantom experiments

To investigate potential differences between rFOV-DWI and c-DWI in more detail, these scans were acquired of water/oil phantoms. The same DWI protocol was used as for the clinical study. As a base measurement, diffusion scans with the two protocols were acquired of sunflower oil contained

in a plastic ball (diameter = 50 mm). The F_0 was set to the frequency of the main CH_2 group plus 420 Hz.

Then the two DWI protocols were acquired of a phantom with a water and oil compartment. A 500 ml glass beaker was filled with 200 ml pineapple juice and then 200 ml of sunflower oil was added to create two adjacent water/oil compartments. Pineapple juice was chosen as a natural aqueous contrast solution, with a T2 matching that of fibro-glandular tissue of approximately 50 ms [11, 12].

Mean ADCs were calculated for ROIs of the whole oil and water components in each slice ($N=12$). A Student's t test was subsequently used on these means, to compare the influence of the acquisition protocol.

Results

For the volunteer study, the SNR of fibro-glandular tissue was 9.7 (number of voxels $N_{\text{voxels}} = 487$) and 18.9 ($N_{\text{voxels}} = 36$) for rFOV-DWI and c-DWI, respectively. The SNR of adipose tissue was 4.4 ($N_{\text{voxels}} = 165$) and 10.4 ($N_{\text{voxels}} = 10$) for rFOV-DWI and c-DWI, respectively.

Patient study

Figure 3A shows the mean ADCs of the 38 lesions for the rFOV protocol versus the conventional protocol. The ADC values of lesions (c-DWI: $1.08 \times 10^{-3} \text{ mm}^2/\text{s}$ (0.60–1.74), rFOV-DWI: $1.13 \times 10^{-3} \text{ mm}^2/\text{s}$ (0.56–1.77)) were not significantly different ($p=0.34$). This also applies to fibro-glandular tissue [$p=0.42$, c-DWI: $1.61 \times 10^{-3} \text{ mm}^2/\text{s}$ (1.01–2.13), rFOV-DWI: $1.57 \times 10^{-3} \text{ mm}^2/\text{s}$ (0.97–2.08)]. The area under

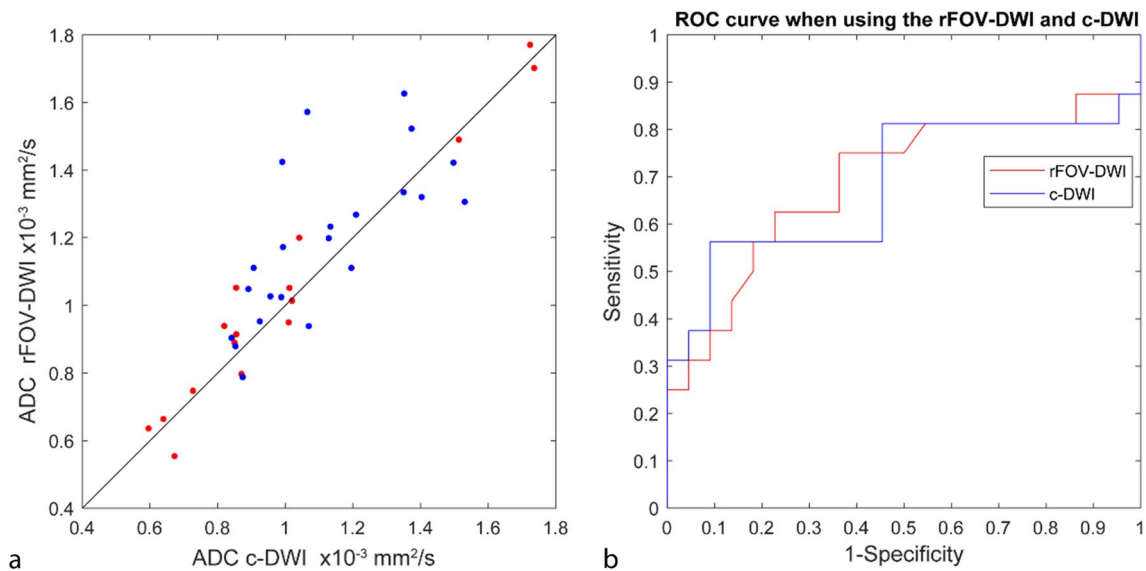


Fig. 3 **a** Mean ADC of lesions with rFOV versus conventional DWI. Blue dots represent benign and red dot malignant lesions. The black line is the $x=y$. **b** ROC curve using the rFOV and conventional protocol.

the curve of the ROC curve for differentiating between malignant and benign lesions (Fig. 3b) was 0.69 and 0.68 for the rFOV and conventional protocol, respectively.

The measured ADC of the adipose tissue using rFOV-DWI had a significantly ($p < 0.002$) higher ADC value than with the conventional DWI protocol. The mean (\pm SD) adipose ADC values with rFOV and the conventional imaging were $0.31 (\pm 0.20) \times 10^{-3} \text{ mm}^2/\text{s}$ and $0.16 (\pm 0.21) \times 10^{-3} \text{ mm}^2/\text{s}$, respectively.

Assessment of Image ghost artifacts

The average artifact score was 2.1 and 2.5 for c-DWI and rFOV-DWI respectively, which was significantly ($p = 0.001$) different. An example of increased ghosting intensity in rFOV-DWI compared with c-DWI is presented in Fig. 4. c-DWI had no score of 4, whereas rFOV-DWI had two cases with a score of 4 both in breasts which visibly appeared to have a large percentage of adipose tissue.

Phantom experiments

For the oil sphere (Fig. 5c), no significant difference ($p = 0.07$) was found in ADCs between the two protocols. For rFOV-DWI, the mean $\text{ADC} = -0.01 (\pm 0.28) \times 10^{-3} \text{ mm}^2/\text{s}$, and for c-DWI, the mean $\text{ADC} = 0.02 (\pm 0.01) \times 10^{-3} \text{ mm}^2/\text{s}$.

Figure 5a, b shows the calculated ADC maps for the water/oil phantom for the rFOV and c-DWI protocols. For both protocols, ghost artifacts were visible (white arrows). A significantly higher (Fig. 5c, $p < 0.001$) ADC of oil was

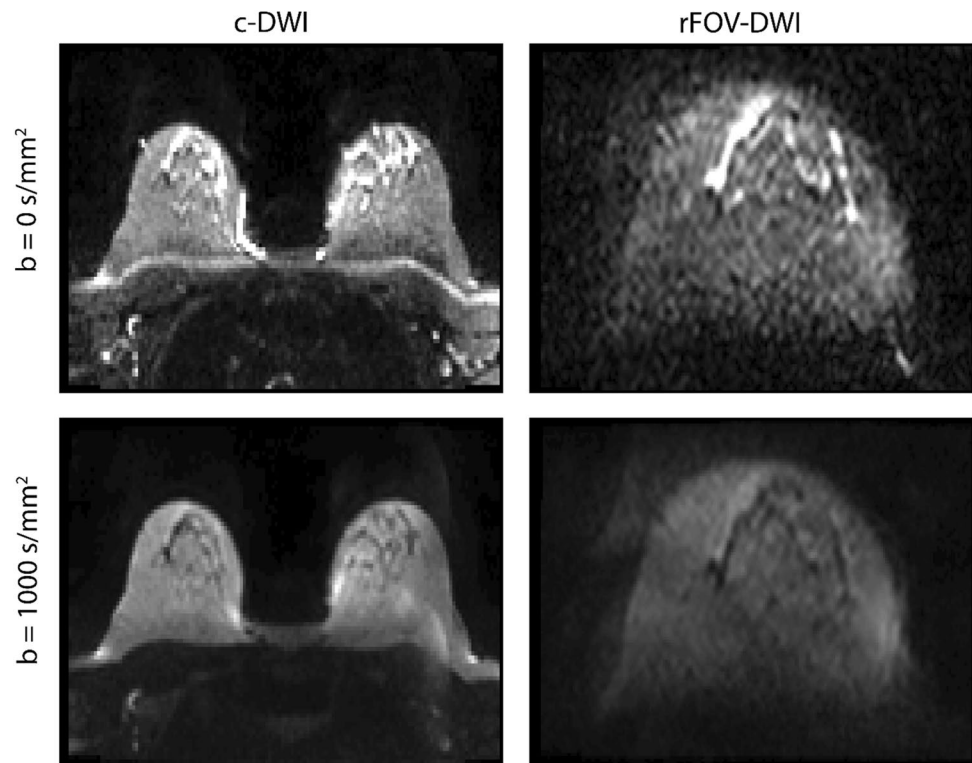
found for rFOV-DWI ($\text{ADC} = 0.18 \times 10^{-3} \text{ mm}^2/\text{s}$) compared to c-DWI ($\text{ADC} = -0.04 \times 10^{-3} \text{ mm}^2/\text{s}$). No significant difference ($p = 0.34$) was found between the ADCs calculated of the water component ($\text{ADC rFOV-DWI} = 1.75 \times 10^{-3} \text{ mm}^2/\text{s}$; $\text{ADC c-DWI} = 1.76 \times 10^{-3} \text{ mm}^2/\text{s}$).

Discussion

In this study, the ADC values obtained with rFOV-DWI imaging were compared to conventional DWI for breast tissue and in an oil/water phantom. No difference was found between the ADCs of tumors and fibro-glandular tissue as measured by the two protocols. These results are consistent with a previous study finding no differences when the mean (malignant) tumor ADC is used [13]. Other studies however reported a lower tumor mean ADC for rFOV-DWI compared with conventional DWI [5, 14, 15]. This difference has been attributed to less partial volume averaging with fibro-glandular and residual fat tissue with the higher-resolution rFOV-DWI and therefore a clearer delineation of the tumor region [13]. In our study, it is possible that difference in exact slice positioning and slice gap between the two protocols caused a greater ADC variation, hiding the influence of in-slice partial volume effects.

For the ADC measurements in adipose tissue and oil, these measurements were essentially of the residual olefinic signal, as the main ‘fat-suppressed’ methylene group had a large water/fat displacement of around 2–3 cm, well known for EPI sequences. The ADC measured in adipose tissue using c-DWI is in the same range ($0.12\text{--}0.54 \times 10^{-3} \text{ mm}^2/\text{s}$)

Fig. 4 Diffusion images showing an example of increased ghosting intensity in rFOV-DWI compared with c-DWI. Images of $b=0, 1000 \text{ s/mm}^2$ pairs are shown with the same window/level settings



as measured by previous studies [16, 17]. A significantly higher ADC was found in adipose tissue for the rFOV-DWI compared to c-DWI.

A possible reason is that the rFOV-DWI has improved fat suppression and thus reveals the small water signal component (blood vessels, organelles) of adipose tissue. However, similar results were found in the water/oil phantom, thus excluding this explanation. Bias in ADC may also result from low SNR [18]. However, rFOV with its higher resolution has a lower SNR compared to c-DWI, and would therefore show a lower measured ADC, not a higher one. Another possible explanation is due to ghost artifacts which appear to be partially present in Fig. 5a, b (white arrows). However, why this appears inhomogeneous for rFOV-DWI, and only influences the ADC of oil for rFOV-DWI and not c-DWI is unclear. Hence, the exact origin of why a higher ADC was found in adipose tissue for rFOV-DWI compared to c-DWI requires further investigation.

Despite the differences in how the ghost artifacts appear in the two protocols, we found no difference in mean lesions' ADC values, and therefore lack of significant clinical impact. This study does suggest that rFOV can be used diagnostically for higher-resolution breast DWI imaging. However, rather than using mean ADC values, measuring other DWI parameters and spatial heterogeneity may be more informative.

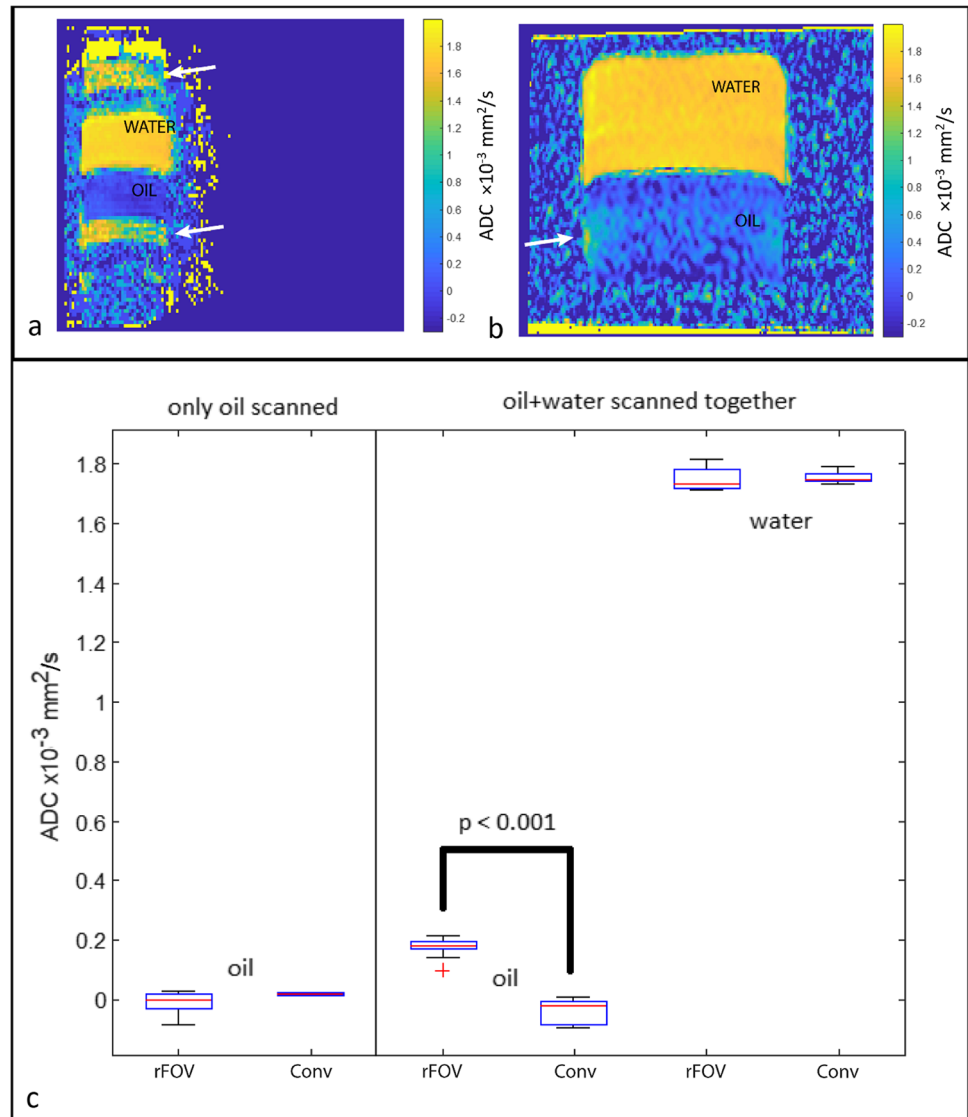
Our study has several limitations. First, the rFOV protocol differed in having both a higher resolution and use of a

2D RF pulse when compared to c-DWI. Too many differences in protocol settings (including TR, TE, and slice gap) can make it more difficult to elucidate the impact of a single setting on the results. However, the protocol was constructed for implementation in the current clinical setting. Additionally, only the mean ADC was measured for the ROIs, while the main clinical advantage of having a higher spatial resolution would be parameters related to the heterogeneity of the region. Because imaging with rFOV-DWI only covers one breast, it would not be suitable for breast cancer screening. Lastly, no noise-floor correction was performed, which may cause bias in the obtained ADC value for the rFOV-DWI protocol for tissue with high ($> 1.6 \times 10^{-3} \text{ mm}^2/\text{s}$) ADC.

This study included both measurements in adipose and fibro-glandular tissue. The inclusion of adipose tissue is unique, as it is mainly a measurement of the olefinic peak, with a frequency (at 3 T) of about 75 Hz separation from the water peak. Given that this residual fat peak has a low intensity with expected ADC close to zero ($< 0.5 \times 10^{-3} \text{ mm}^2/\text{s}$), it could function as a sensitive internal probe to image quality difference, including artifacts, between DWI protocols. This is in fact what we have observed, highlighting differences between the protocols, that would otherwise have been overlooked. For future DWI comparison studies, including measurements in adipose tissue is therefore recommended.

To conclude, this study found no significant difference in the ADCs of fibro-glandular tissue and lesions when using rFOV-DWI compared to c-DWI, despite the higher

Fig. 5 ADC maps obtained with **a** conventional DWI and **b** rFOV-DWI. The arrows indicate ghost artifacts. **c** Box whisker plots of the ADC's for oil and water for the left-side: oil-only scan, and right side: water/oil phantom



resolution and more accurate ROIs in the rFOV method. Ghost artifacts appeared to have a greater influence on the measured ADC when using rFOV, as detected in adipose regions. These artifacts however appeared to have no influence on the measured ADC of aqueous tissue.

Data Availability The datasets used and/or analyzed during the current study are available from the corresponding author on reasonable request.

Declarations

Conflict of interest The authors declare that they have no conflict of interest.

Ethical standard This is a prospective institutional review board approved study.

References

1. Rieseberg S, Frahm J, Finsterbusch J (2002) Two-dimensional spatially-selective RF excitation pulses in echo-planar Imaging. *Magn Reson Med* 47(6):1186–1193
2. Schneider Evaluation of 2DRF Echo-Planar Pulse Designs for Parallel Transmission. In: ISMRM, 2012.
3. Mei CS, Panych LP, Yuan J, McDannold NJ, Treat LH, Jing Y, Madore B (2011) Combining two-dimensional spatially selective RF excitation, parallel imaging, and UNFOLD for accelerated MR thermometry imaging. *Magn Reson Med* 66(1):112–122
4. Katscher U, Bornert P, Leussler C, van den Brink JS (2003) Transmit sense. *Magn Reson Med* 49(1):144–150
5. Dong HB, Li YD, Li H, Wang B, Hu B (2014) Study of the reduced field-of-view diffusion-weighted imaging of the breast. *Clin Breast Cancer* 14(4):265–271
6. Saritas EU, Cunningham CH, Lee JH, Han ET, Nishimura DG (2008) DWI of the spinal cord with reduced FOV single-shot EPI. *Magn Reson Med* 60(2):468–473

7. Tamada T, Ream JM, Doshi AM, Taneja SS, Rosenkrantz AB (2017) Reduced field-of-view diffusion-weighted magnetic resonance imaging of the prostate at 3 tesla: comparison with standard echo-planar imaging technique for image quality and tumor assessment. *J Comput Assist Tomo* 41(6):949–956
8. Chen MZ, Feng C, Wang QX, Li JL, Wu SS, Hu DY, Deng BD, Li Z (2021) Comparison of reduced field-of-view diffusion-weighted imaging (DWI) and conventional DWI techniques in the assessment of Cervical carcinoma at 3.0T: Image quality and FIGO staging. *Eur J Radiol* 137.
9. von Morze C, Kelley DAC, Shepherd TM, Banerjee S, Xu DA, Hess CP (2010) Reduced field-of-view diffusion-weighted imaging of the brain at 7 T. *Magn Reson Imaging* 28(10):1541–1545
10. Thierfelder KM, Sommer WH, Dietrich O, Meinel FG, Theisen D, Paprottka PM, Strobl FF, Pfeuffer J, Reiser MF, Nikolaou K (2014) Parallel-transmit-accelerated spatially-selective excitation MRI for reduced-FOV diffusion-weighted-imaging of the pancreas. *Eur J Radiol* 83(10):1709–1714
11. Arthurs OJ, Graves MJ, Edwards AD, Joubert I, Set PAK, Lomas DJ (2014) Interactive neonatal gastrointestinal magnetic resonance imaging using fruit juice as an oral contrast media. *BMC Med Imaging* 14.
12. Rakow-Penner R, Daniel B, Yu HZ, Sawyer-Glover A, Glover GH (2006) Relaxation times of breast tissue at 1.5T and 3T measured using IDEAL. *J Magn Reson Imaging* 23(1):87–91.
13. Singer L, Wilmes LJ, Saritas EU, Shankaranarayanan A, Proctor E, Wisner DJ, Chang B, Joe BN, Nishimura DG, Hylton NM (2012) High-resolution diffusion-weighted magnetic resonance imaging in patients with locally advanced breast cancer. *Acad Radiol* 19(5):526–534
14. Barentsz MW, Taviani V, Chang JM, Ikeda DM, Miyake KK, Banerjee S, van den Bosch MA, Hargreaves BA, Daniel BL (2015) Assessment of tumor morphology on diffusion-weighted (DWI) breast MRI: diagnostic value of reduced field of view DWI. *J Magn Reson Imaging* 42(6):1656–1665
15. Wilmes LJ, McLaughlin RL, Newitt DC, Singer L, Sinha SP, Proctor E, Wisner DJ, Saritas EU, Kornak J, Shankaranarayanan A, Banerjee S, Jones EF, Joe BN, Hylton NM (2013) High-resolution diffusion-weighted imaging for monitoring breast cancer treatment response. *Acad Radiol* 20(5):581–589
16. Baron P, Dorrius MD, Kappert P, Oudkerk M, Sijens PE (2010) Diffusion-weighted imaging of normal fibroglandular breast tissue: influence of microperfusion and fat suppression technique on the apparent diffusion coefficient. *NMR Biomed* 23(4):399–405
17. Englander SA, Ulug AM, Brem R, Glickson JD, van Zijl PC (1997) Diffusion imaging of human breast. *NMR Biomed* 10(7):348–352
18. Dietrich O, Heiland S, Sartor K (2001) Noise correction for the exact determination of apparent diffusion coefficients at low SNR. *Magn Reson Med* 45(3):448–453

Publisher's Note Springer Nature remains neutral with regard to jurisdictional claims in published maps and institutional affiliations.

Springer Nature or its licensor (e.g. a society or other partner) holds exclusive rights to this article under a publishing agreement with the author(s) or other rightsholder(s); author self-archiving of the accepted manuscript version of this article is solely governed by the terms of such publishing agreement and applicable law.